

Exploring the X-ray and γ -ray properties of the redback millisecond pulsar PSR J1723-2837

C. Y. Hui¹, P. H. T. Tam², J. Takata³, A. K. H. Kong², K. S. Cheng³, J. H. K. Wu², L. C. C. Lin⁴ and E. M. H. Wu³

ABSTRACT

We have investigated the X-ray and γ -ray properties of the redback millisecond pulsar PSR J1723-2837 with *XMM-Newton*, *Chandra* and *Fermi*. We have discovered the X-ray orbital modulation of this binary system with the minimum that coincides with the phases of radio eclipse. The X-ray emission is clearly non-thermal in nature which can be well described by a simple power-law with a photon index of ~ 1.2 . The phase-averaged luminosity is $\sim 9 \times 10^{31}$ erg/s in 0.3-10 keV which consumes $\sim 0.2\%$ of the spin-down power. We have detected the γ -ray emission in 0.1 – 300 GeV from this system at a significance of $\sim 6\sigma$ for the first time. The γ -rays in this energy range consumes $\sim 2\%$ of the spin-down power and can be modeled by a power-law with a photon index of ~ 2.6 . We discuss the high energy properties of the new redback in the context of an intrabinary shock model.

Subject headings: gamma rays: stars — Pulsars: individual (PSR J1723-2837)
— X-rays: binaries

1. Introduction

Alpar et al. (1982) proposed that a millisecond pulsar (MSP) is formed as an old neutron star spun-up by accreting matter from its binary companion. Since the first MSP was discovered ~ 30 years ago (Backer et al. 1982), dedicated pulsar surveys have resulted in a population of more than two hundred MSPs which comprise $\sim 10\%$ of the whole radio

¹Department of Astronomy and Space Science, Chungnam National University, Daejeon 305-764, Korea

²Institute of Astronomy and Department of Physics, National Tsing Hua University, Hsinchu, Taiwan

³Department of Physics, University of Hong Kong, Pokfulam Road, Hong Kong

⁴General Education Center, China Medical University, Taichung 40402, Taiwan

pulsar population known today (cf. Manchester et al. 2005). Despite the large sample size, many details of how an accretion-powered X-ray binary evolves into a rotation-powered pulsar remained missing.

While MSPs are expected to be the end products of the X-ray binary evolution, $\sim 20\%$ of the known MSPs are found to be isolated (Roberts 2013). One popular scenario to explain their solitudes is the high energy radiation and/or the pulsar wind particles from these rejuvenated pulsars have ablated their companions. This suggested scenario was motivated by the discovery of the first “black widow” MSP PSR B1957+20 which has a very low mass companion ($M_c \sim 0.02M_\odot$) in a 9.2-hr orbit (Fruchter, Stinebring & Taylor 1988). A recent X-ray investigation of this system has demonstrated that the orbital modulation is due to the intra-binary shock emission between the pulsar wind and the ablated material from the companion star (Huang et al. 2012).

More than a dozen of black widow MSPs have been found in the Galactic field, which are characterized by their tight orbits $P_b \lesssim 20$ hrs, existence of eclipse and a very low companion mass $M_c \lesssim 0.05M_\odot$ (Roberts 2013). These systems probably have already left the stage of transiting from a X-ray binary to a MSP. In the last few years, a new population of MSPs started to emerge which has established a missing link for this transition. PSR J1023+0038 is the first object that confirms such a link (Archibald et al. 2009). This pulsar was previously known as a low mass X-ray binary (Homer et al. 2006) and pulsations in radio and X-ray band were subsequently discovered (Archibald et al. 2009). Also, the accretion disk that previously found in this system has disappeared since 2002 (Wang et al. 2009; Archibald et al. 2009, 2010). Its companion is non-degenerate with a mass of $\sim 0.2M_\odot$ is also found to be higher than the end-point mass for its orbital period ($P_b \sim 4.8$ hr) expected from various binary evolution models (Tauris & Savonije 1999; cf. Fig. 1 in Roberts 2013). X-ray orbital modulation and γ -ray emission have also been detected from this system (Tam et al. 2010).

Currently, more than a dozen systems with characteristics similar to PSR J1023+0038 have been identified so far.⁵ These system are suggested to be in a bi-stable state which can possibly swing between rotation and accretion power phases according to the rate of Roche lobe overflow. This scenario has been recently confirmed by the observed switches between these two states in PSR J1824-2452I on a very short timescale (Papitto et al. 2013). All these systems are dubbed as “redbacks”.

PSR J1723-2837, which is one of these redbacks, has its radio and optical properties been recently reported (Crawford et al. 2013). Its rotational period and orbital period are 1.86 ms and 14.8 hr respectively. The spin-down luminosity of the pulsar is determined as

⁵see <http://apatruno.wordpress.com/about/millisecond-pulsar-catalogue/> for updated information.

$\dot{E} = 4.6 \times 10^{34}$ erg s⁻¹. The mass of its companion lies in a range of $0.4 - 0.7M_{\odot}$ and optical spectroscopy indicates it is a G-type star. The pulsar follows a nearly circular orbit. The eclipse of radio pulses takes $\sim 15\%$ of the orbit which twice the Roche lobe size inferred for the companion (Crawford et al. 2013). In this Letter, we report the results from our X-ray and γ -ray analysis of this system.

2. Observation & Data Analysis

2.1. *XMM-Newton* observations

PSR J1723-2837 has been observed by *XMM-Newton* on 3 March 2011 for a total exposure of ~ 56 ks with all EPIC cameras operated in full frame mode (Obs. ID: 0653830101). With the updated instrumental calibrations, we generated all the event files with XMM Science Analysis Software (XMMSAS version 12.0.1). We subsequently selected only the data in the energy range of $0.3 - 10$ keV and those events correspond to the pattern in the range of $0 - 12$ for MOS1/2 cameras and $0 - 4$ for the PN camera. Bad pixels were also excluded. The effective exposures for MOS1, MOS2 and PN after filtering are found to be ~ 50.7 ks, ~ 49.6 ks and ~ 49.3 ks respectively. Within a source region of 20 arcsec radius around the pulsar timing position (RA= $17^{\text{h}}23^{\text{m}}23.1856^{\text{s}}$ Dec= $-28^{\circ}37'57.17''$ (J2000)), there are 4993 cts, 3655 cts and 13261 cts (source+background) extracted from MOS1, MOS2 and PN CCDs respectively. All the EPIC data are found to be unaffected by CCD pile-up.

We firstly searched for the orbital modulation in X-ray. Before any temporal analysis performed, we have applied barycentric correction to the arrival times of all the events by using the updated planetary ephemeris JPL DE405. Then we subtracted the background in the individual camera by adopting an annular region with inner/outer radius of 25 arcsec/45 arcsec centered at the pulsar position. Using the radio ephemeris for PSR J1723-2837 (Tab. 2 in Crawford et al. 2013), we folded the background-subtracted light curves at the orbital period. The X-ray modulation can be clearly seen with all three cameras. In order to improve the photon statistics, we combine all the EPIC data and the resultant folded light curve is shown in the upper panel of Figure 1. We adopted the time of ascending node (MJD 55425.320466) to be the epoch of phase zero. Due to the incomplete orbital coverage after data filtering, there is gap at the orbital phase interval $0.14 - 0.18$ in this *XMM-Newton* data.

The minimum of the X-ray orbital modulation occurs at the same phase interval that radio eclipse has been observed (cf. Fig. 1 in Crawford et al. 2013) which is illustrated by the shaded region in Figure 1. This interval encompasses the inferior conjunction (INFC) at

a phase of ~ 0.25 where the pulsar is behind its companion. Apart from the region around INFC, radio observations at 2 GHz also could not detect the pulsar in the phase interval of $0.5 - 0.6$ which might indicate the presence of an extended companion wind that is driven by the pulsar (Crawford et al. 2013). However, in examining the X-ray orbital modulation at this interval, we cannot identify any peculiar behavior.

On the other hand, the maximum of the modulation is found in the orbital phase interval of $0.7 - 0.9$ (see Fig. 1). In this interval, we have found a dip at the superior conjunction (SUPC) near a phase of ~ 0.8 .

For investigating its X-ray spectral properties, we extracted the source and background spectra from the same regions adopted in the temporal analysis. We grouped the spectrum obtained from each camera dynamically so as to obtain the same signal-to-noise ratio in each data set. All the data are fitted simultaneously to the tested models. All the uncertainties quoted in this paper are 1σ for 2 parameters of interest (i.e. $\Delta\chi^2 = 2.3$).

First, we have examined the phase-averaged X-ray spectrum of PSR J1723-2837. We found that a simple absorbed power-law model can describe the observed spectral data reasonably well ($\chi^2 = 171.84$ for 179 d.o.f). The best-fit model yields a column density of $N_H = 2.31_{-0.25}^{+0.28} \times 10^{21} \text{ cm}^{-2}$, a photon index of $\Gamma_X = 1.19 \pm 0.05$ and a normalization of $1.10_{-0.07}^{+0.08} \times 10^{-4} \text{ photons keV}^{-1} \text{ cm}^{-2} \text{ s}^{-1}$ at 1 keV. The best-fit N_H is consistent with the value inferred from the optical extinction $A_V = 1.2$ of this system (Crawford et al. 2013; Predehl & Schmitt 1995). The unabsorbed energy flux in $0.3 - 10 \text{ keV}$ is $f_x = 1.32_{-0.16}^{+0.19} \times 10^{-12} \text{ erg cm}^{-2} \text{ s}^{-1}$. At a distance of 0.75 kpc, this corresponds to an X-ray luminosity of $L_x \sim 8.9 \times 10^{31} \text{ erg s}^{-1}$. For the tested thermal model, they are not able to provide any adequate description of the data.

We proceeded to investigate if the spectral properties vary at different orbital phases. We have extracted the spectra from two phase ranges, $0.2-0.4$ and $0.7-0.9$ which encompass INFC and SUPC respectively. For the INFC interval, the best-fit yields an $N_H = 2.94_{-1.25}^{+2.30} \times 10^{21} \text{ cm}^{-2}$ and $\Gamma_X = 1.23_{-0.19}^{+0.32}$. On the other hand, the corresponding parameters for the SUPC interval are estimated as $N_H = 2.01_{-0.43}^{+0.49} \times 10^{21} \text{ cm}^{-2}$ and $\Gamma_X = 1.09 \pm 0.09$. Within the statistical uncertainties, the spectral parameters inferred in these two intervals are consistent with the phase-averaged values. Hence, we conclude that there is no convincing evidence for the orbital-dependent X-ray spectral behavior found from this data.

2.2. *Chandra* observation

Chandra observed PSR J1723-2837 with the Advanced CCD Imaging Spectrometer

(ACIS) on 2012 July 11 with an effective exposure of 49.9 ks (ObsID: 13713). The ACIS was operated with a sub-array mode to achieve a timing resolution of 0.4s. Similar to the *XMM-Newton* observation, we performed barycentric correction to the arrival times of all the events by using the updated planetary ephemeris JPL DE405. PSR J1723-2837 is clearly seen and is the brightest source in the image. In order to reduce the background, we limited our analysis in the 0.3–7 keV band. Using a circular source region with a radius of 4 arcsec, there are 4468 counts for subsequent analysis. An annulus source free region centered at PSR J1723-2837 was used for background subtraction.

We extracted the 0.3–7 keV lightcurve of PSR J1723-2837; like the *XMM-Newton* observation, the 14.8-hr orbital modulation is clearly seen (see Fig. 1). Although the number of counts is much less than that of *XMM-Newton*, the lightcurve profile is consistent with the *XMM-Newton*'s one. It is worth noting that there is a hint for the dip at phase ~ 0.8 seen in the *XMM-Newton*. We therefore conclude that this feature is genuine.

For spectral analysis, we first investigated the phase-averaged spectrum. The spectrum can be well described ($\chi^2 = 186.85$ for 204 d.o.f) with an absorbed power-law model with $N_H = (1.68 \pm 0.34) \times 10^{21} \text{cm}^{-2}$ and $\Gamma_X = 1.00 \pm 0.07$. The unabsorbed 0.3–10 keV flux is $1.64 \times 10^{-12} \text{ erg cm}^{-2} \text{ s}^{-1}$. The spectrum of *Chandra* is only slightly harder than that of *XMM-Newton*. Since PSR J1723-2837 is bright for *Chandra*, some pile-up may contaminate the spectral analysis. We also included a pile-up model and found that the pile-up fraction is only 1.7% and the spectral parameters are more or less the same. We then performed a phase-resolved spectroscopy using the same phase bins for INFC and SUPC as in the *XMM-Newton* data. Both spectra can be fit with an absorbed power-law. For INFC, the best fit is $N_H = (3.51_{-1.15}^{+1.42}) \times 10^{21} \text{cm}^{-2}$ and $\Gamma_X = 1.35 \pm 0.22$, while for SUPC the corresponding parameters are $N_H = (1.3 \pm 1.0) \times 10^{21} \text{cm}^{-2}$ and $\Gamma_X = 0.82 \pm 0.17$. Like in the *XMM-Newton* data, there is no evidence for orbital dependent spectral variability.

2.3. *Fermi* observations

The γ -ray data used in this work were obtained between 2008 August 4 and 2013 July 15, available at the Fermi Science Support Center ⁶. We used the Fermi Science Tools v9r31p1 package to reduce and analyze the Pass7 data in the vicinity of PSR J1723-2837. To reduce the contamination from Earth albedo γ -rays, we excluded events with zenith angles greater than 100° . We used events with energies between 100 MeV and 300 GeV in the binned likelihood analysis. Data that are classified as the “source” events were used.

⁶<http://fermi.gsfc.nasa.gov/ssc/>

The corresponding instrument response function was used.

We chose a square region of dimension $28^\circ \times 28^\circ$ centered on the radio timing position as our region-of-interest (ROI). We subtracted the background contribution by including the Galactic diffuse model (`gal_2yearp7v6_v0.fits`) and the isotropic background (`iso_p7v6source.txt`), as well as all sources in the second Fermi/LAT catalog (2FGL; Nolan et al. 2012) within the circular region of 25° radius around the γ -ray position. We assumed the respective spectrum in the 2FGL catalog for all the sources considered. The normalization of the diffuse components and spectral parameter values of sources within 5° from PSR J1723-2837 were allowed to vary.

Using the “source” events and assuming a power-law spectrum at the pulsar position, the maximized test-statistic (TS) value (Mattox et al. 1996) we obtained for the PSR J1723-2837 position is 38.3, corresponding to a detection significance of 6.2σ . The power-law index is $\Gamma_\gamma = 2.6 \pm 0.1$. The photon flux from the power-law fit is $(3.5 \pm 0.7) \times 10^{-8}$ photons $\text{cm}^{-2} \text{s}^{-1}$, and the energy flux is $(1.5 \pm 0.3) \times 10^{-11}$ erg $\text{cm}^{-2} \text{s}^{-1}$, corresponding to the γ -ray luminosity of 10^{33} erg s^{-1} at a distance of 0.75 kpc, or 2% of the spin-down luminosity. A fit using a power-law with an exponential cutoff did not provide a satisfactory fit. We also chose different ROIs to verify our results.

Given the proximity of PSR J1723-2837 to the Galactic Center region where the Galactic γ -ray diffuse background is high, we also performed a binned likelihood analysis using “clean”-class events in a smaller ROI of dimension $21^\circ \times 21^\circ$ centered on the radio timing position. The TS value thus obtained is 24.2, corresponding to a detection significance of 4.9σ . Taking into account the above likelihood results using “source” events and “clean” events, we believe that the detection of the γ -ray source is robust.

Crawford et al. (2013) estimated the γ -ray efficiency to be $<0.7\%$, based on the non-detection of any γ -ray source from the direction of PSR J1723-2837 in the second Fermi catalog (Nolan et al., 2012). They quote an upper limit of the energy flux from PSR J1723-2837 to be the minimum point-source flux in the Galactic plane, i.e., 5×10^{-12} erg $\text{cm}^{-2} \text{s}^{-1}$. In fact, the minimum detectable flux in the region around PSR J1723-2837 should be much higher, due to its proximity to the Galactic Center. As shown in this work, the γ -ray energy flux is $(1.5 \pm 0.3) \times 10^{-11}$ erg $\text{cm}^{-2} \text{s}^{-1}$.

To better estimate the γ -ray position, we performed an unbinned analysis of the front-converted “clean”-class events larger than 500 MeV with the aid of *gtfindsrc*, resulting in the position at $\text{RA}(J2000)=260:906$, $\text{Dec}(J2000)=-28:631$, with statistical uncertainty 0.13° at the 68% confidence level, which is consistent with the position of PSR J1723-2837. The background-subtracted count map of the $2^\circ \times 2^\circ$ region centered on the radio position, con-

structured using the “clean” class events, is shown in Figure 3.

To search for possible γ -ray variability related to the orbital modulation, we divided the photons into two phase-intervals, one centered at the SUPC (0.5-1.0), the other centered at the INFC (0.0-0.5), and performed likelihood analysis for each group of photons. No difference of the spectral parameters were found between SUPC and INFC. We also searched for the periodic signals by using H -test (de Jager & Büsching 2010). Neither the γ -ray periodicity related to the orbital period nor the rotation period obtained from the radio ephemeris of PSR J1723-2837 was found in this analysis.

3. Summary & Discussion

Using *XMM-Newton* and *Chandra* data, we found a strong X-ray orbital period of PSR J1723-2837. In addition, we discovered the γ -ray emission of PSR J1723-2837 for the first time by using *Fermi*. The orbital modulation of the X-ray emissions from PSR J1723-2837 suggests the emission processes in the intra-binary space, because the magnetospheric emissions will not modulate with the orbital phase. This is very similar to another redback, 1FGL J2339.7-0531 (Kong et al. 2012). The eclipsing radius $\sim R_\odot$ of the pulsed radio emissions is significantly larger than the Roche-lobe radius, indicating existing the Roche-lobe overflow from the companion star (Crawford et al. 2013). The interaction of the cold-relativistic pulsar wind with the outflow from the companion will produce a shock, and the pulsar wind particles will be randomized and accelerated at the shock. The shocked pulsar wind particles will emit X-rays through the synchrotron radiation. We can in principle constrain the magnetization parameter and the Lorentz factor of the cold-relativistic pulsar wind with the observed non-thermal emissions from the redback pulsars. With a simple one-dimensional model (Takata et al. 2012), we discuss how the pulsar wind parameters of PSR J1723-2837 are constrained.

Since the radio eclipse lasts only 15% of its orbit, we expect the shock wraps the companion star and its distance from the pulsar is on the order of the semi-major axis, which is $a \sim 3.7 \times 10^{10} / \sin i$ cm, where i is the orbital inclination angle and it is $i \sim 30^\circ - 41^\circ$ for PSR J1723-2837. The radio eclipse also suggests the angle of flow from the companion star measured from the pulsar is $\theta_a \sim 2\pi \times 0.15 = 0.94$. If the pulsar wind is emitted spherically then the fraction of the pulsar wind stopped by the outflow is $\sim 5\%$. The magnetic fields upstream (B_1) and behind (B_2) the shock are estimated as $B_1 \sim (L_{sd}\sigma/a^2c)^{1/2}$ and $B_2 = 3B_1$, where σ is the ratio of the magnetic energy to kinetic energy of the cold relativistic pulsar wind and is to be assumed a value smaller than unity (i.e. kinetically dominated flow). At the shock, the pulsar wind particles are accelerated beyond the Lorentz factor

(Γ_1) of the cold relativistic pulsar wind in the upstream region. For the maximum Lorentz factor of the accelerated particles, it is determined by balancing the accelerating time scale, $\tau_{acc} \sim \Gamma m_e c / (eB_2)$, and the synchrotron cooling time scale, $\tau_s \sim 9m_e^3 c^5 / (4e^4 B^2 \Gamma)$.

The observed X-ray photon index $\Gamma_X \sim 1.2$ may imply the power law index of the particle distribution at the shock is $p \sim 1.4$. For the usual power law index $p \sim 2 - 2.5$ of the shock acceleration, this hard photon index in the spectrum will be reproduced if the typical synchrotron energy (E_1) of the minimum Lorentz factor Γ_1 is larger than 10 keV. The photons index changes from $\alpha = (p + 1)/2$ above E_1 to $\alpha = 3/2$ below E_1 . In such a case, the X-ray emission properties break the degeneracy of σ and Γ_1 in the emission model. For example, we can fit the observed properties $\alpha \sim 1.2$ and $f_x \sim 1.3 \times 10^{-12} \text{erg cm}^{-2} \text{s}^{-1}$ with $(\sigma, \Gamma_1) \sim (0.1, 5 \times 10^4)$. The predicted Lorentz factor $\Gamma_1 \sim 5 \times 10^4$ is similar to those of the original black widow pulsar PSR B1957+20 (Wu et al. 2012).

Because PSR J1723-2837 follows an almost circular orbit, the shock distance from the pulsar does not vary across the orbit, suggesting the spectral properties of the intrinsic shock emissions do not modulate with the orbital phase. The variation of the observed flux will be caused by either Doppler boosting effect with a mildly relativistic flow of the shocked flow or physical eclipse of the emission region. However, these two effects will not produce a significant variation in the spectrum. The observed amplitude (see Figure 1) implies the Doppler factor is $\sim 1 - 2$, which does not cause a significant change in the spectral shape. Furthermore, because the synchrotron cooling time scale of the particles that emit photons of energies < 10 keV is longer than crossing time scale of the system, the distribution of the particles does not evolve within the orbit. Therefore, the spectral shape of the X-ray emission in 0.3-10 keV from various parts of the orbit should be the same. Even the partial region of the emission region is covered by the star, the observed spectral shape is the same with that for whole emission regions.

For black widow/redback pulsars, the magnetospheric emissions and pulsar wind emissions produce the GeV gamma-rays. For the original black widow pulsar PSR B1957+20, Wu et al. (2012) suggested both the magnetospheric and the pulsar wind emissions contribute to the GeV emissions found by the *Fermi*. With the results described in section 2.3, it is unclear which process operates for the observed gamma-rays for PSR J1723-2837, because neither pulsar's spin period nor orbital modulation was founded in the current *Fermi* data. However, a single power-law feature in the observed spectrum in 0.1-300 GeV band suggests the origin of the pulsar wind. In such a case, the synchrotron radiation process explains the observed emissions around 100MeV and the inverse-Compton process off the stellar photons contributes to the emissions above ~ 10 GeV.

The shocked particles that emit the synchrotron photons will produce TeV photons

through the inverse-Compton off the stellar photons, for which the effective temperature is $T_{eff} \sim 4800 - 6000\text{K}$. Based on the calculation with the isotropic photon fields, we can estimate the flux above $> 100\text{GeV}$ as $F_{>100\text{GeV}} \sim 5 \times 10^{-13}\text{erg cm}^{-2} \text{s}^{-1}$, which will be possible to be measured by the future observations of the Cherenkov Telescope Array.

CYH is supported by the National Research Foundation of Korea through grant 2011-0023383. PHT is supported by the National Science Council of the Republic of China (Taiwan) through grant NSC101-2112-M-007-022-MY3. JT and KSC are supported by a GRF grant of HK Government under HKU7009 11P. AKHK is supported by the National Science Council of the Republic of China (Taiwan) through grant NSC100-2628-M-007-002-MY3 and NSC100-2923-M-007-001-MY3. LCCL is supported by the National Science Council through grants NSC 101-2112-M-039-001-MY3.

REFERENCES

- Alpar, M. A., Cheng, A. F., Ruderman, M. A., & Shaham, J. 1982, *Nature*, 300, 728
- Archibald, A. M., et al. 2010, *ApJ*, 722, 88
- Archibald, A. M., et al. 2009, *Science*, 324, 1411
- Backer, D. C., Kulkarni, S. R., Heiles, C., Davis, M. M., & Goss, W. M. 1982, *Nature*, 300, 615
- Crawford, F., et al. 2013, *ApJ*, 776, 20
- de Jager, O. C., Büsching, I. 2010, *A&A*, 517, L9
- Fruchter, A. S., Stinebring, D. R., & Taylor, J. H. 1988. *Nature*, 333, 237
- Homer, L., et al. 2006, *AJ*, 131, 562
- Huang, R. H. H., et al. 2012, *ApJ*, 760, 92
- Kong, A. K. H. et al. 2012, *ApJ*, 747, L3
- Manchester, R. N., et al. 2005, *AJ*, 129, 1993
- Mattox, J. R., et al. 1996, *ApJ*, 461, 396
- Nolan, P. L., et al. 2012, *ApJS*, 199, 31

Papitto, A., et al. 2013, *Nature*, 501, 517

Predehl, P., & Schmitt, J. H. M. M. 1995, *A&A*, 293, 889

Roberts, M. S. E. 2013, *Proceedings of the International Astronomical Union*, Volume 291, pp. 127-132

Takata, J., et al. 2012, *ApJ*, 750, 70

Tam, P. H. T., Hui, C. Y., Huang, R. H. H., et al. 2010, *ApJ*, 724, L207

Tauris, T. M., & Savonije, G. J. 1999, *A&A*, 350, 928

Wong, Z. et al. 2009, *ApJ*, 703, 2017

Wu, E. M. H., et al. 2012, *ApJ*, 761, 181

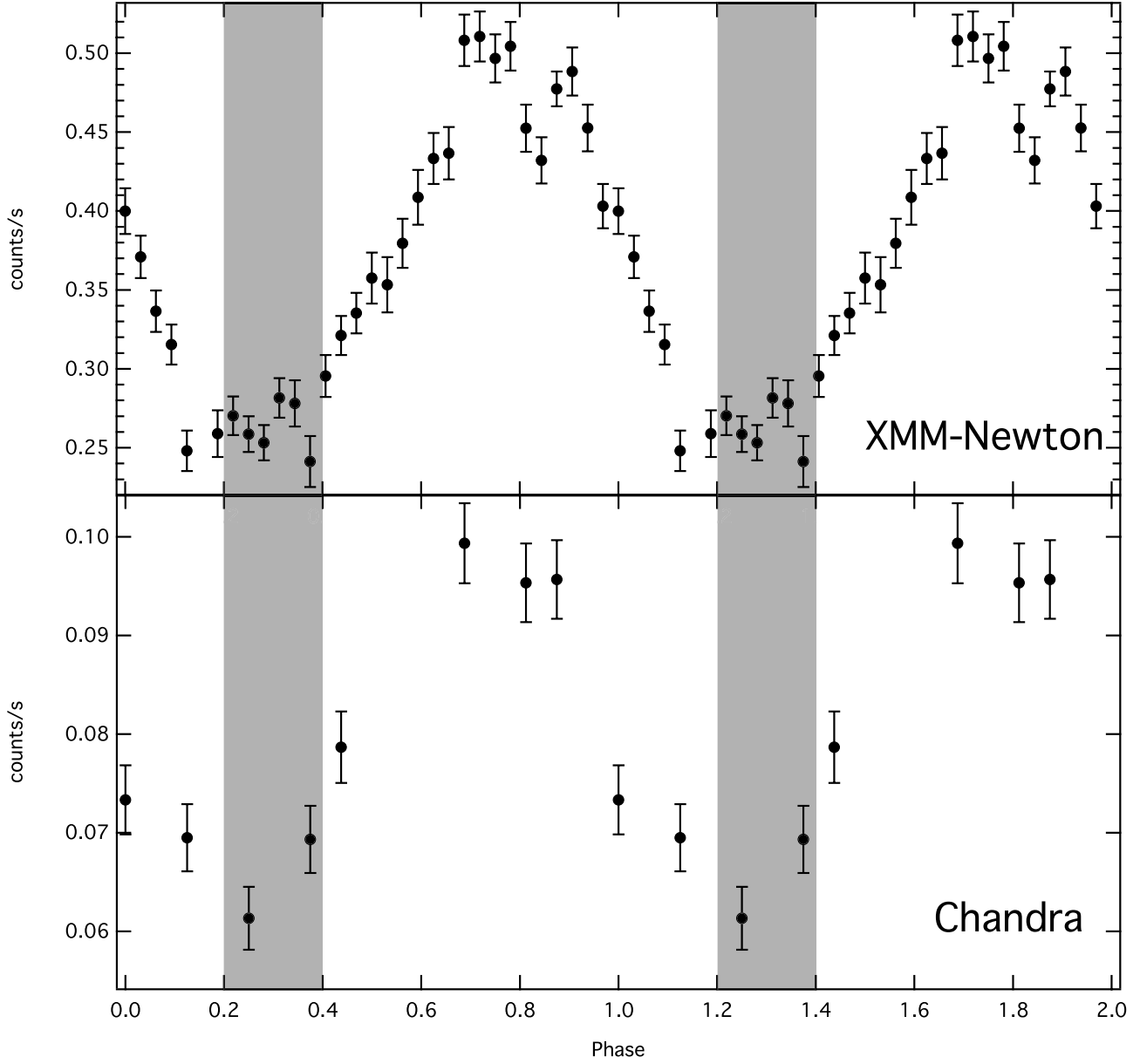


Fig. 1.— The background-subtracted light curves of PSR J1723-2837 as observed by *XMM-Newton* in 0.3 – 10 keV with the data from all EPIC cameras combined (*upper panel*) and by *Chandra* ACIS in 0.3 – 7 keV (*lower panel*). Two periods of orbital motion are shown for clarity. The shaded region illustrates the phase interval of the radio eclipse.

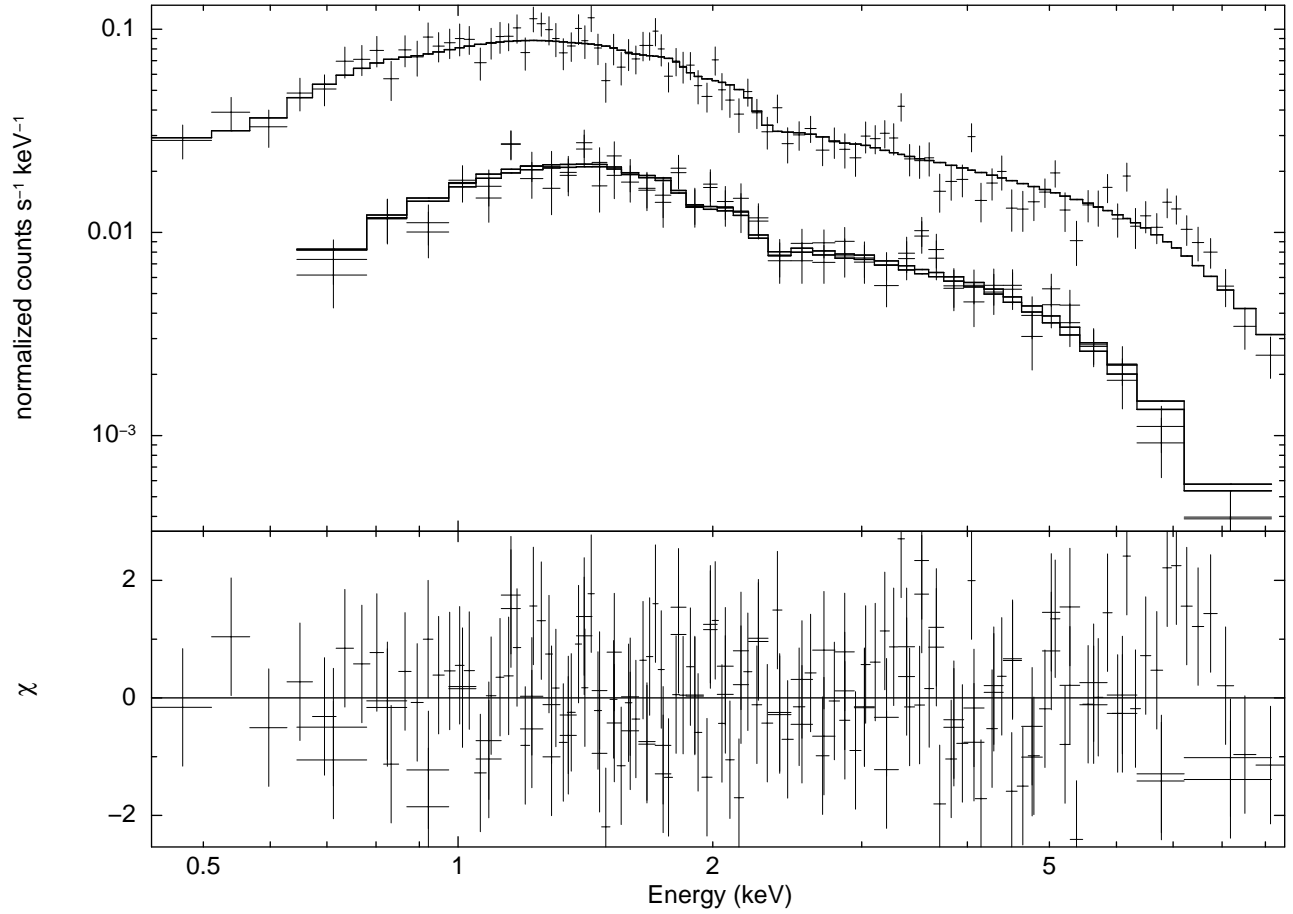


Fig. 2.— The phase-averaged X-ray spectra of PSR J1723-2837 as observed by *XMM-Newton* and simultaneously fitted to an absorbed power-law model (upper panel) and contribution to the χ^2 -fit statistic (lower panel).

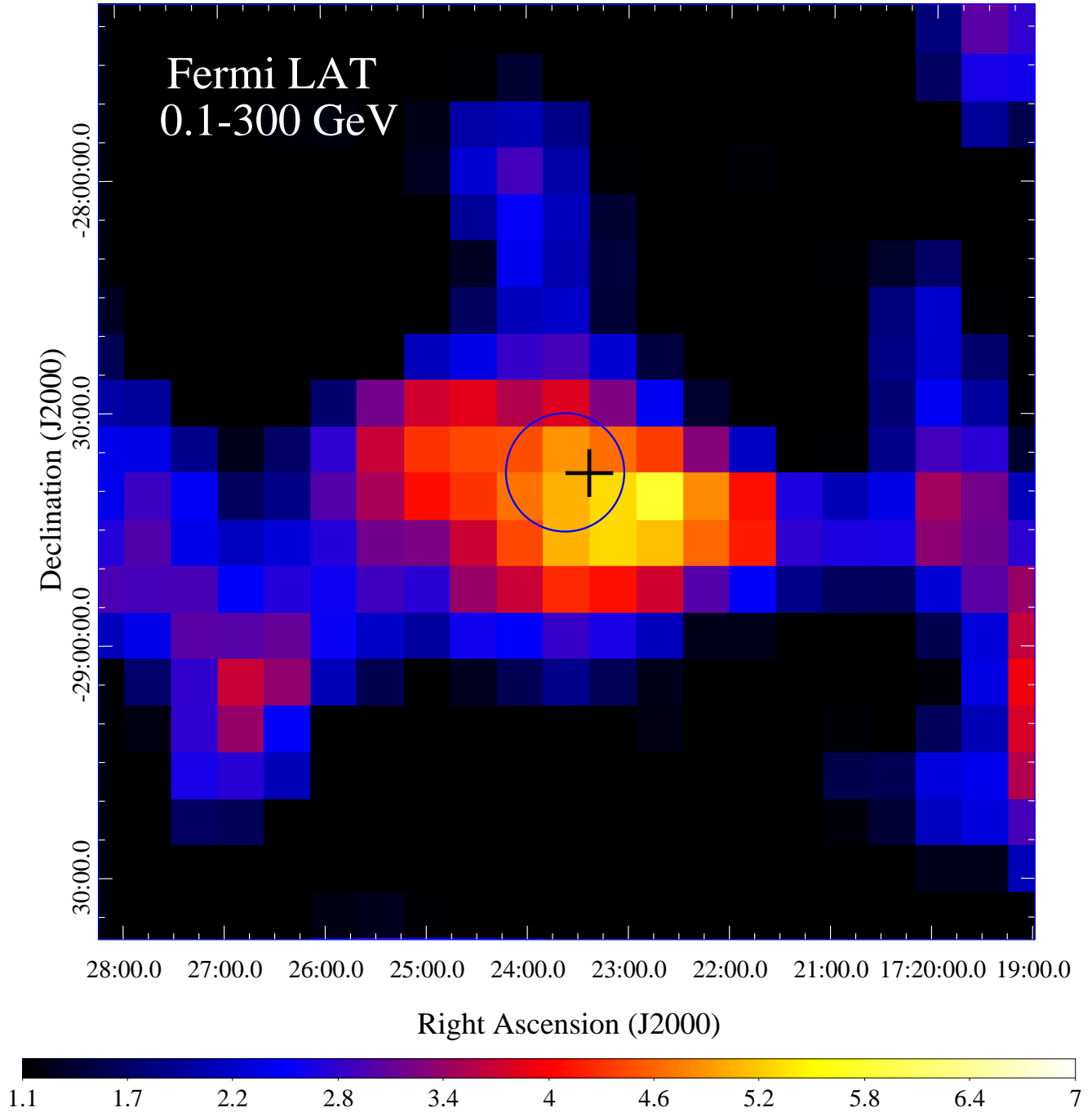


Fig. 3.— The background-subtracted 0.1–300 GeV γ -ray count map, smoothed with a Gaussian width of $0\text{.}3^\circ$, of the $2^\circ \times 2^\circ$ region centered on PSR J1723-2837, whose radio timing position is indicated by the black cross. The blue circle indicates the error circle of the best-fit position at the 68% confidence-level (see text).